

We are IntechOpen, the world's leading publisher of Open Access books Built by scientists, for scientists

6,900

Open access books available

185,000

International authors and editors

200M

Downloads

Our authors are among the

154

Countries delivered to

TOP 1%

most cited scientists

12.2%

Contributors from top 500 universities



WEB OF SCIENCE™

Selection of our books indexed in the Book Citation Index
in Web of Science™ Core Collection (BKCI)

Interested in publishing with us?
Contact book.department@intechopen.com

Numbers displayed above are based on latest data collected.
For more information visit www.intechopen.com



Multilayered Nanostructures Integrated with Emerging Technologies

Maria L. Braunger, Rafael C. Hensel, Gabriel Gaál, Mawin J.M. Jimenez, Varlei Rodrigues and Antonio Riul Jr

Abstract

Surface and interface functionalization are crucial steps to introduce new functionalities in numerous applications, as faster dynamics occur on surfaces rather than bulk. Within this context, the layer-by-layer (LbL) technique is a versatile methodology to controllably form organized nanostructures from the spontaneous adsorption of charged molecules. It enables the assembly of multilayered LbL films on virtually any surface using non-covalent molecular interactions, allowing the nanoengineering of interfaces and creation of multifunctional systems with distinct building blocks (polymers, clays, metal nanoparticles, enzymes, organic macromolecules, etc.). Several applications require thin films on electrodes for sensing/biosensing, and here we explore LbL films deposited on interdigitated electrodes (IDEs) that were 3D-printed using the fusing deposition modeling (FDM) technique. IDEs covered with LbL films can be used to form multisensory systems employed in the analysis of complex liquids transforming raw data into specific patterns easily recognized by computational and statistical methods. We extend the FDM 3D-printing methodology to simplify the manufacturing of electrodes and microchannels, thus integrating an e-tongue system in a microfluidic device. Moreover, the continuous flow within microchannels contributes to faster and more accurate analysis, reducing the amount of sample, waste, and costs.

Keywords: LbL assembly, interdigitated electrodes, microchannel, 3D printing, electrical measurements, e-tongue

1. Introduction

In 1966, Iler proposed the deposition of multilayered films through the consecutive adsorption of charged inorganic colloids [1]. In 1997, Decher and coworkers extended Iler's method in an even more general approach using the spontaneous physical adsorption of materials from aqueous solutions [2]. It enables the assembly of layer-by-layer (LbL) nanostructured thin films on solid supports using a wide variety of building blocks (DNA, enzymes, proteins, polymers, inorganic particles, clays, colloids, etc.). The widespread use of the LbL technique in numerous applications has led to the development of conventional procedures that were organized in five distinct categories [3, 4]: immersive, spin, spray, electromagnetic, and fluidic assemblies. **Figure 1** shows a simplified schematic diagram of the LbL immersive

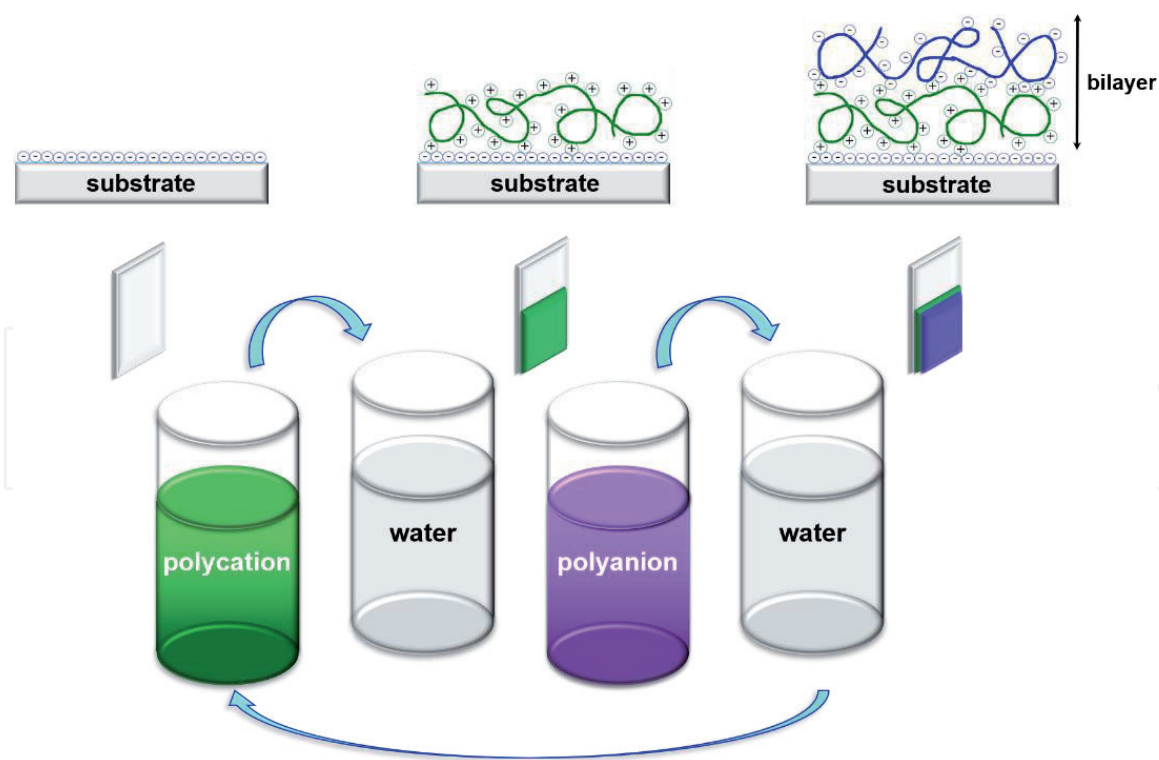


Figure 1.
Schematic representation of the LbL immersive assembly and the formation of the first cationic/anionic bilayer.

assembly and the consecutive bilayer formation. Briefly, a solid substrate is dipped in an aqueous dispersion containing the material to be adsorbed. Subsequently, the substrate is rinsed to remove loosely bound material, allowed to dry, and then immersed in another polyelectrolyte solution of opposite charge. Then, multilayered thin films are formed by spontaneously alternating the adsorption between cationic and anionic layers.

There are a myriad of LbL applications in the literature [5], being electronic tongues (e-tongue) a quite interesting example of nanostructures used in the analysis of liquid samples through specific pattern recognition by computational and statistical methods. In 2016, Alessio et al. applied a microfluidic e-tongue based on LbL films to evaluate different coffee brands [6]. The results demonstrated the device's ability to distinguish selected gourmet, organic, and premium coffees from unselected grains. In 2017, Daikuzono et al. also used LbL films in a microfluidic e-tongue setup to detect gliadin (a gluten protein) in order to evaluate gluten-containing foodstuff [7]. Authors were able to detect trace amounts of gliadin in ethanol solutions (up to 0.005 mg kg^{-1}) using computational analysis (Interactive Document Map, IDMAP), detecting also the contamination of gluten-free foodstuff with gliadin, paving the way for the detection in real-life situations.

Salvo-Comino et al. have used LbL films fabricated by spin-coating process and electrochemical characterization in milk analysis [8]. They have used LbL architectures based on chitosan (CHI), 1-butyl-3-methylimidazolium tetrafluoroborate (IL), copper(II) tetrasulfonated phthalocyanines (CuPc^{S}), and galactose oxidase (GAO). Two identical LbL CHI+IL/ CuPc^{S} architectures were made, with the GAO enzyme deposited on top of one of them. The formed biosensor enabled the distinction of milk samples having different lactose contents. Authors also compared Principal Component Analysis (PCA) results with Partial Least Squares (PLS-1) models, obtaining extra information from the milk samples.

LbL films have also been employed in environmental monitoring, aiming the detection of water, air, or soil contamination. In 2017, Barros et al. used

Square-Wave Anodic Stripping Voltammetry (SWASV) using indium tin oxide (ITO) electrodes functionalized with LbL films for the detection of trace levels of cadmium (Cd^{2+}), lead (Pb^{2+}), and copper (Cu^{2+}) [9]. The incorporation of AuNPs in LbL structures composed by emeraldine salt polyaniline (PANi-ES) and sodium montmorillonite clay mineral (Na^+MMT) enhanced the electrocatalytic response of the sensors to heavy metal ions, achieving a lower detection limit (from mgL^{-1} to μgL^{-1}). Also in 2017 Andre et al. tested hybrid LbL films as gas sensor to detect ammonia (NH_3) in hazardous pollutant monitoring [10]. LbL films composed by polyaniline (PANi), graphene oxide (GO), and zinc oxide (ZnO) were combined in a tetralayered structure (PANi/GO/PANi/ZnO) onto gold interdigitated electrodes (IDEs). The best performance in NH_3 detection using impedance spectroscopy was achieved with three tetralayers. Two years later, Rodrigues et al. have used LbL films of graphene nanoplatelets and AuNPs in the detection of methyl parathion [11], a highly toxic organophosphorus ester insecticide according to the World Health Organization [12]. The electrochemical results showed the successful detection of methyl parathion in real samples, such as tap water, soil, and cabbage.

LbL films have also been applied for diagnosis in medical and pharmaceutical areas. In 2018, de Lucena et al. tested composite LbL films on the electrochemical detection of dopamine in the presence of natural interferents such as ascorbic acid and uric acid [13]. The limit of detection (LOD) obtained was consistent with those found in the literature for other LbL architectures, with a higher range of detection ($5\text{--}150 \mu\text{mol L}^{-1}$). In 2019, Camilo et al. proposed the synthesis of AuNP conjugated to anti-PSA (prostate-specific antigen) antibody to produce a label-free impedimetric immunosensor based on LbL architectures [14]. The film was assembled onto gold electrodes previously modified with a thiol monolayer, followed by the deposition of an LbL framework incorporating biological materials for specific PSA detection. A LOD of 0.17 ng mL^{-1} was achieved without demanding secondary antibodies, reducing costs, and pointing out to a high potential in the actual detection of prostate cancer. In 2009, Silva et al. applied sensors based on LbL films in the detection of cholesterol in egg yolks, with high potential for food analysis and diet management [15]. Cholesterol oxidase (ChOx) was immobilized on the top of the LbL films composed by conventional polyelectrolytes, gold nanoparticles, and carbon nanotubes, with the sensor first tested to detect and evaluate the cholesterol concentration in commercial solutions and later in food samples by monitoring amperometric signals.

Tunable properties of the LbL films were reported by Fontinele et al. using Norbixin (NBx), a carotenoid extracted from urucum [16]. They have fabricated (NBx/PANi) LbL composite films onto ITO substrates, enabling an electrochemically stable charge transfer. That was possible as the presence of NBx in the film architecture did not inhibit PANi conductive characteristics. Cortez et al. showed highly organized LbL structures of lipid-like surfactants and polyelectrolytes, a distinct feature of the normally obtained “fuzzy” formation from polycation-polyanion multilayer assemblies [17]. LbL films fabricated with poly(allylamine) hydrochloride (PAH) and sodium dodecyl phosphate (DP) displayed a well-stratified layer formation and highly oriented lamellar structures, with X-ray data revealing the presence of Bragg peaks up to fourth order, an interesting configuration for applications requiring naturally ordered spacers in a nacre-like structure.

Here, we will focus on multilayered thin films to form multifunctional coatings and the application of the 3D-printing technique as an alternative methodology for fast prototyping and design of sensors. The emerging 3D-printing technique also enabled an easy integration with other research areas such as microfluidics.

2. Alternative techniques and materials for sensor development

In this section we will describe some subjects and methodologies involved in the development of multilayered nanostructures used in sensory analysis.

2.1 Alternative materials for electrodes

2.1.1 3D-printed interdigitated electrodes

IDEs are a category of planar parallel plate capacitor formed by two metallic combs facing each other. It is a powerful tool for sensing and biosensing owing to the high sensitivity of getting small signal variations close to the IDEs' surface, being widely explored in impedimetric e-tongues used in the analysis of complex liquid systems. Traditional photolithography and microfabrication processes are usually employed in the manufacture of IDEs, enabling the fabrication at the micrometer range. However, it demands multistep processes, specialized facilities, trained personnel, and the use of toxic and expensive reagents. However, in the last decade ink-jet and 3D-printing technologies have emerged as alternative methods for simpler fabrication of electrodes using nonconventional conductive materials [18–20].

3D-printed electrodes are built up typically at the submillimeter range due to limitations imposed by nozzles; nonetheless, the technique has attracted considerable attention due to the fast prototyping, use of alternative materials, and reduction steps in the fabrication of complex geometries within a few minutes. It generally comes straight from the computer screen, with no need of photomasks and intermediate microfabrication steps that usually take a couple of hours using conventional techniques. The materials used as conductive tracks are also attractive because they can be readily deposited onto flexible substrates and integrated with organic and soft electronics [18]. Within this milieu of fast and automated prototyping, the Fused Deposition Modeling 3D printing (FDM) technique shows great potential to fabricate a conductive electrode pattern in a one-step process within minutes. FDM uses thermoplastic filaments to build up the construct, with many commercial materials available to be exploited in the fabrication of devices [21, 22]. To illustrate, conductive filaments enable the manufacture of electrodes, while conventional filaments can be used to board the body of the device. It is possible to prototype the whole electrode in a single printing process if someone uses a multifilament FDM printer, thus increasing the flexibility in the buildup of complex structures with a reduced fabrication time [23]. Recently, a homemade dual-extruder FDM printer was used to fabricate macro planar IDEs and sensor body in e-tongue applications. Each sensing unit was printed within 8 minutes having good reproducibility in the fabrication process of conventional e-tongue devices [24].

2.1.2 Transparent conductive electrodes

Transparent conductive electrodes are indispensable components for potential applications in optoelectronic devices, such as solar cells, flexible displays, light emitting diodes, and touch screens [25–28]. Materials with high transmittance and adequate electrical conductivity are desired in such applications [29]; therefore, the most commonly used material is indium tin oxide (ITO) due to its good optical and electrical properties (e.g., transmittance~80% at visible wavelength and low sheet resistance $<40 \Omega/\text{sq}$) [30]. However, ITO is brittle by nature limiting flexible applications [31] and presents~75% indium in its composition, which might hamper display and optoelectronic uses due to its scarcity and increasing cost [32]. Many new

transparent conductive materials have been developed to circumvent this problem, including hybrid/composites and multilayered thin films [33–36]. However, some transparent electrodes have complicated structures or require complex processing, demanding the search for new strategies to produce transparent conductive materials at low-cost and with a compatible upscale production.

Many expectations were placed on graphene as a prominent material for the next generation of electronics due to its unique properties derived from the honeycomb configuration of carbon atoms placed in a one-atom thick sheet having sp^2 hybridizations [37]. However, pristine graphene is a semimetallic material having a null bandgap that limits its use in some devices. Graphene has been mostly obtained from chemical vapor deposition (CVD), however, with the cost of a nontrivial separation/transfer process of the produced graphene layers, as the CVD growth is generally made on copper substrates. The separation process can seriously compromise the quality of the graphene samples, and the chemical synthesis of reduced graphene oxide (rGO) appears as a promising alternative. It enables a large scale production, and rGO has properties resembling pristine graphene, with an adjustable bandgap from structural defects and the presence of oxygenated groups in its structure [38]. The presence of oxygen at the basal plane allows the functionalization of the material with polymers and biomolecules, expanding its use with other techniques and enhancing potential applications [39, 40]. The control of dimensionality, quantum confinement, and edge effects is an important factor defining the electronic properties in graphene derivatives [41]. Within this context, the LbL assembly is an elegant way to control both thickness and molecular architecture of rGO structures at nanoscale, potentiating the use of graphene-based materials in flexible electronics, sensors, biosensing, transparent electrodes, and energy storage devices [42–44].

In the last decade, several studies were conducted to study the properties of rGO nanoplatelets (two-dimensional material) as well as zero-dimensional graphene quantum dots (GQDs) [45, 46]. However, there are still scarce studies on the electrical properties and behavior of charge carriers in nanostructured LbL films. Recently, we have shown that multilayered rGO films allowed a fine-tuning on both optical and electrical properties (**Figure 2**). The formation of nanocomposites from rGO chemically functionalized with sodium polystyrene sulfonate (PSS), named here as GPSS and also as quantum dots (GPSS:QDs) or nanoplatelets (GPSS:NPLs), with poly(diallyldimethylammonium chloride) (PDPA), enabled an intraplanar 2D conduction mechanism due to the confinement of charge carriers within the

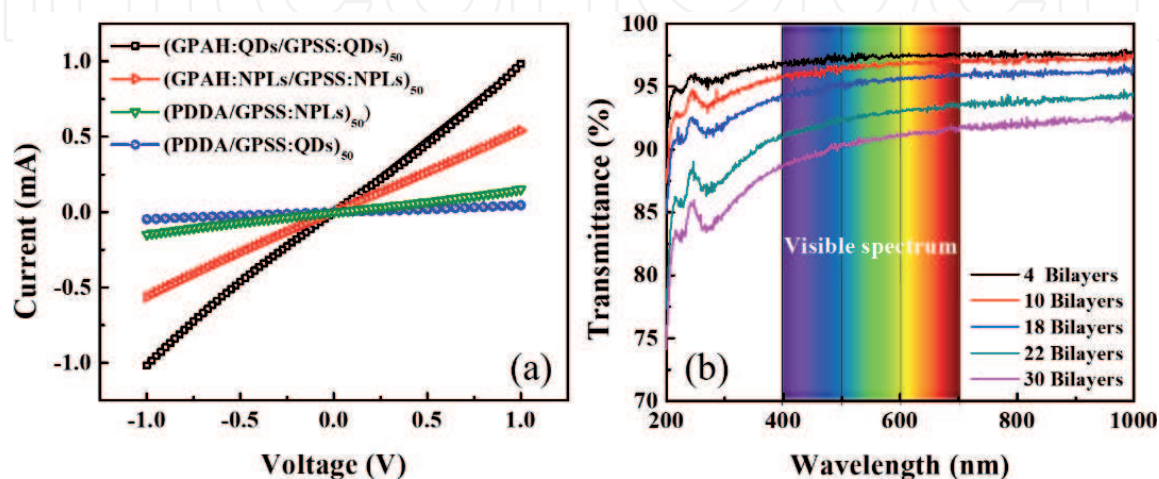


Figure 2
 (a) I-V measurements for different LbL films of rGO deposited onto gold interdigitated electrodes.
 (b) Transmittance spectra of (GPAH:QDs/GPSS:QD)_n LbL film.

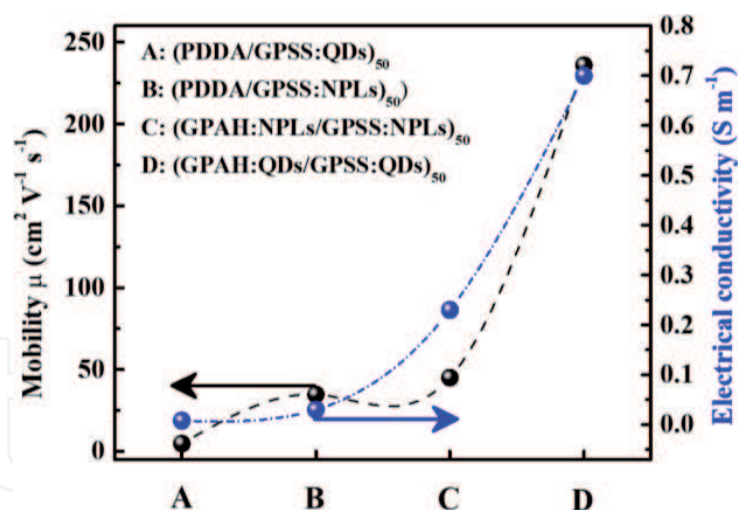


Figure 3.

Mobility of charge carriers and electrical conductivity of different LbL architectures formed mainly by rGO.

conductive layers formed by GPSS in the PDDA/GPSS LbL assembly. **Figure 2a** shows current vs. voltage (I-V) curves from distinct rGO LbL architectures. A strong dependence of the electrical properties with the size of the rGOs is clearly seen [38, 47, 48]. The (GPAH:QDs/GPSS:QDs)_n LbL film, being *n* the number of deposited bilayers, displayed high transmittance (from 89–92% in the visible region for *n* = 30), as shown in **Figure 2b**.

Notable differences were observed in the mobility of charge carriers depending on the size of the nanoplatelets involved in the LbL film formation being, respectively, $4.7 \text{ cm}^2 \text{V}^{-1} \text{s}^{-1}$ for (PDDA/GPSS:QDs)₅₀ and $34.7 \text{ cm}^2 \text{V}^{-1} \text{s}^{-1}$ for (PDDA/GPSS:NPLs)₅₀ [47]. Nevertheless, higher mobility values could be achieved exploring synergistic size effects in the LbL assembly formed only by rGOs, either as quantum dots (QDs) or nanoplatelets (NPLs). That was reached changing PDDA in the LbL structures by rGO wrapped with poly(allylamine hydrochloride) (PAH), named here as GPAH. The (GPAH:QDs/GPSS:QD) LbL film exhibited high mobility values ($\mu = 236 \text{ cm}^2 \text{V}^{-1} \text{s}^{-1}$) [48], with changes illustrated in **Figure 3**. The improvement in the electrical characteristics was attributed to rGO size effects, with a 3D driving mechanism assisted mainly by phonons when in QD form. The successful achievement of multilayered rGO:QDs films presenting high transmittance and noticeable mobility values paves the way for future applications in high performance, low-cost optoelectronic devices.

2.2 Film growth monitored by electrical measurements

Electrolyte-insulator-semiconductor (EIS) electrochemical capacitors are charged sensitive devices detecting charge variation at electrolyte-insulator interfaces [49]. They are widely applied in the monitoring of electrical features during the LbL film growth [50, 51]. Briefly, the electrical behavior of (PAH/PSS) LbL films on EIS devices is characterized by a zigzag-like capacitance behavior after each adsorption step, attributed to the outermost charge layer alternation [52]. Furthermore, a similar behavior was also observed in C-V measurements preserving the capacitance constant after each adsorbed layer onto the EIS sensor [53]. However, EIS devices work in salt medium, and such environmental condition certainly modifies the electrical properties in LbL structures. As a simple alternative, IDEs can be used to analyze the LbL films properties in air or in water, with no need of salt addition. However, experimental methods were developed to avoid the influence of aqueous medium on the electrical characterization of LbL films

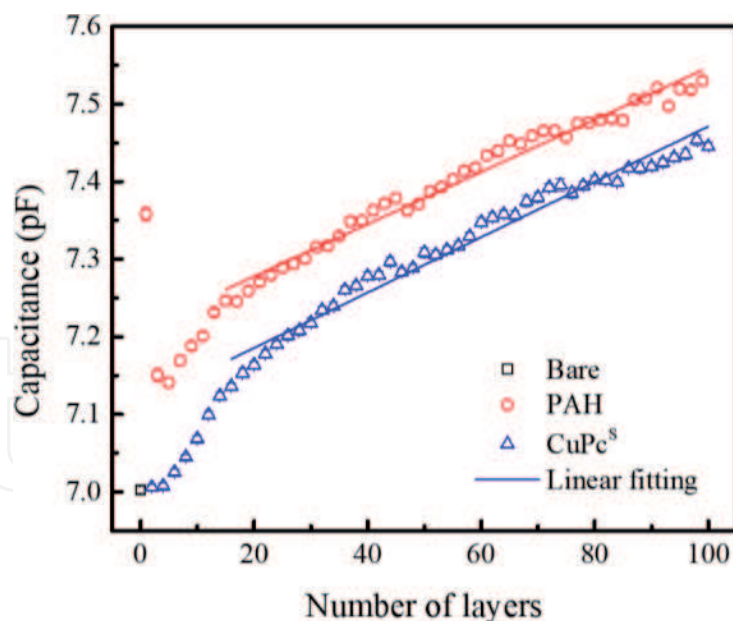


Figure 4. Capacitance variation as a function of the number of adsorbed layers. Dark square corresponds to the bare IDE, red circles to capacitance measurements after PAH adsorption, and blue triangles after CuPc^S adsorption.

[47, 54]. **Figure 4** presents the capacitance variation after the deposition of each PAH or copper phthalocyanine (CuPc^S) adsorbed layer, followed by spontaneous drying onto gold IDEs. A capacitance alternation according to the outermost deposited layer (PAH or CuPc^S) due to charge overcompensation was observed. For measurements performed in air, the amplitude of the capacitance alternation did not depend on the number of deposited layers, a consequence of the charge density after each deposited PAH layer. In addition, **Figure 4** presents a linear trend after the 16th adsorbed layer of both polyelectrolytes, which was associated with the replacement of an air layer on the top of the IDE by the LbL film, thus increasing the dielectric constant near the IDEs surface. Accordingly, the observed linearity was associated with the deposition of the same amount of material after each adsorption step. Therefore, it allows for the evaluation of both appropriate material and thickness selection for a desired application based on the electrical measurements performed in the LbL film growth.

2.3 Incorporation of nanoparticles by physical methods

The selection of materials having desired functionalities can tune properties in LbL assemblies, such as superhydrophobicity [55], ionic permeability [56], electrical conductivity [57], etc. As an example, the incorporation of gold nanoparticles into LbL films composed by PANi and Na⁺MMT enabled the electrochemical detection of trace levels of cadmium, lead, and copper ions [9]. The inclusion of gold nanoparticles increased also the discrimination between skimmed, semi-skimmed, and full-fat milk samples [58]. Although the deposition of nanoparticles between layers in LbL structures might increase both sensitivity and selectivity [9, 58], it is not possible to control an adequate dispersion of them during the spontaneous adsorption process. Consequently, it precludes a better comprehension of the influence of nanoparticles on enhanced sensitivity and selectivity. An alternative is the use of physically prepared metal nanoparticles to assembly samples by independently controlling size, concentration, and distribution of nanoparticles free of surfactants at interfaces. To illustrate, palladium nanoparticles were successfully implanted in poly(methyl methacrylate), effectively modifying

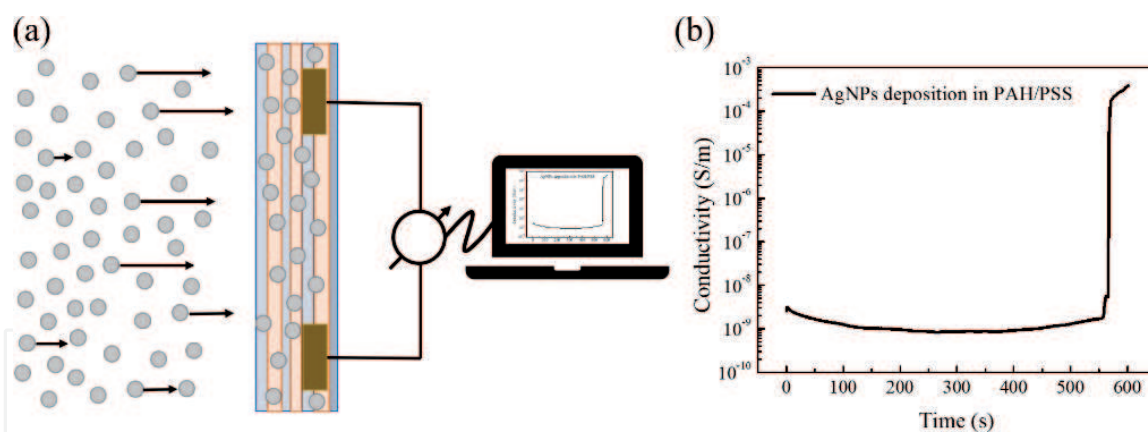


Figure 5. (a) Scheme to illustrate in situ conductivity monitoring of nanoparticle deposition into LbL films onto IDE. Note the scheme presents just a pair of digits to facilitate viewing. (b) Electrical conductivity variation of PAH/PSS LbL films 200 nm thick onto gold IDEs during the deposition of Ag nanoparticles.

the electrical properties of the polymer in a specific region [59]. In this context, we have incorporated 3 nm silver nanoparticles preformed in the gas phase into (PAH/PSS) LbL films. The silver nanoparticles were formed in an atomic cluster source, mass-selected using ionic optics, with in situ analysis of their size by a time of flight mass spectrometer (TOF) [60]. Then, the mass-selected silver nanoparticles were deposited in (PAH/PSS)_n LbL films previously deposited onto gold IDEs. **Figure 5** illustrates the electrical changes in the LbL film during the nanoparticles' deposition. Initially, tiny variations on the electrical characteristics that were associated with the insertion of charged nanoparticles in the LbL film structure were observed. An increase in the nanoparticle's concentration created conductive pathways in the LbL films, thus increasing the conductivity four orders of magnitude after reaching a percolation limit. Therefore, independent control on nanoparticles' deposition in a surfactant-free process allowed a better comprehension of their influence in the physicochemical properties of hybrid LbL nanostructures.

2.4 Multifunctional materials

Intrinsic self-healing materials have received great attention in the last decade due to the recovery of mechanical properties after damage through reversible dynamic covalent and non-covalent interactions [61]. Distinct building blocks and strategies have been extensively investigated to enable a reliable, functional healing as some polymers involved in the process are vulnerable to abrasion. Again, the LbL technique is as a powerful tool in the buildup of multifunctional interfaces based on spontaneous non-covalent interactions of materials, tuning the interface characteristics [62–64]. Such interactions introduce properties not exhibited by individual materials, which can be easily exemplified with polyethylenimine (PEI) and poly(acrylic acid) (PAA). The materials individually do not present self-regeneration; therefore, when combined in (PEI/PAA) LbL architectures, the intrinsic self-healing capability appears after ~30 deposited bilayers, as the first deposited layers are strongly compromised in interactions with the substrate [65, 66]. The healing ability can also be controlled by changing the pH, salt concentration, and temperature during the deposition process due to changes in the polymer configuration [67]. The film properties can also be tuned by post-deposition treatments or by adding fillers to the polyelectrolytes. Chen et al. showed that after the deposition process, one can freeze-dry the PEI/PAA film in order to create microporous structures inside the interface,

which were then loaded with drug solutions by wicking or adsorption method [68]. By adding water to the film, the porous structures were healed, and the drug was kept inside the film that was later used to create a controlled drug delivery system.

2.5 Electronic tongue devices

Aiming the integration of the FDM 3D-printing technology in e-tongue devices, microchannels were printed onto gold IDEs having 30 pairs of digits separated 40 μm away from each other, 3 mm in length and 40 μm in width. The electrodes were previously manufactured by photolithography on transparency sheets, and polylactic acid (PLA) was chosen to fabricate the microchannels due to its relative transparency when printed in thin layers, facilitating the flow visualization inside microchannels. The deposition of the IDEs on thin transparency sheets was planned to promote a better sealing with the 3D-printed PLA microchannel (**Figure 6a**). A functional integrated e-tongue device was then developed combining both photolithography and 3D-printing technologies, with LbL films deposited onto the IDEs to form distinct sensing units inside the 3D-printed microchannels (**Figure 6b**). After long usage in repetitive experiments, the detachment of the IDEs inside the microchannels was observed. Although the device was not as robust as conventional ones with IDEs manufactured on glass slides, it can be easily used in fast analysis [22] requiring disposable devices.

Traditional soil chemical investigation is an expensive and time-consuming process, thus motivating the development of alternative approaches in precision agriculture [69–71]. Recently, we have used an e-tongue system based on impedance spectroscopy to recognize different soil samples enriched with macronutrients [24, 72]. Initially, it was used a traditional PDMS microchannel sealed onto gold IDEs fabricated on glass substrates by photolithography (**Figure 7a**). After that, it was used an e-tongue system with 3D-printed IDEs using graphene-based polylactic acid filaments (**Figure 7b**). The sensing units were fabricated using the same materials to facilitate additional comparisons.

The e-tongue systems were tested checking their capability to distinguish soil samples individually enriched with N, P, K, Ca, Mg, and S nutrients, delivered to the soil via chemical fertilizers. The soil samples were simply diluted in water and measured using electrical impedance spectroscopy, with raw data analyzed by PCA. **Figure 8** presents the PCA plot obtained from both devices. Although the results are visually not identical, it is possible to note in both cases a clear distinction of all soil samples tested in PCA plots. A cluster between control and P soil

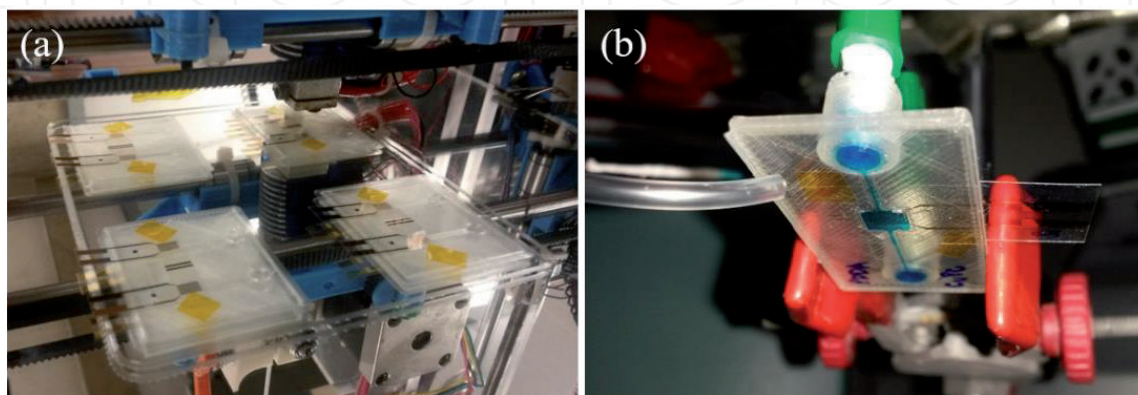


Figure 6.
(a) PLA microchannels while printing by FDM onto transparency sheets and (b) mixed device formed by 3D-printed microchannel and IDE previously manufactured by photolithography. In blue the deposition of the CuPc^S layer in an LbL film structure is evidenced (PDDA/CuPc^S).

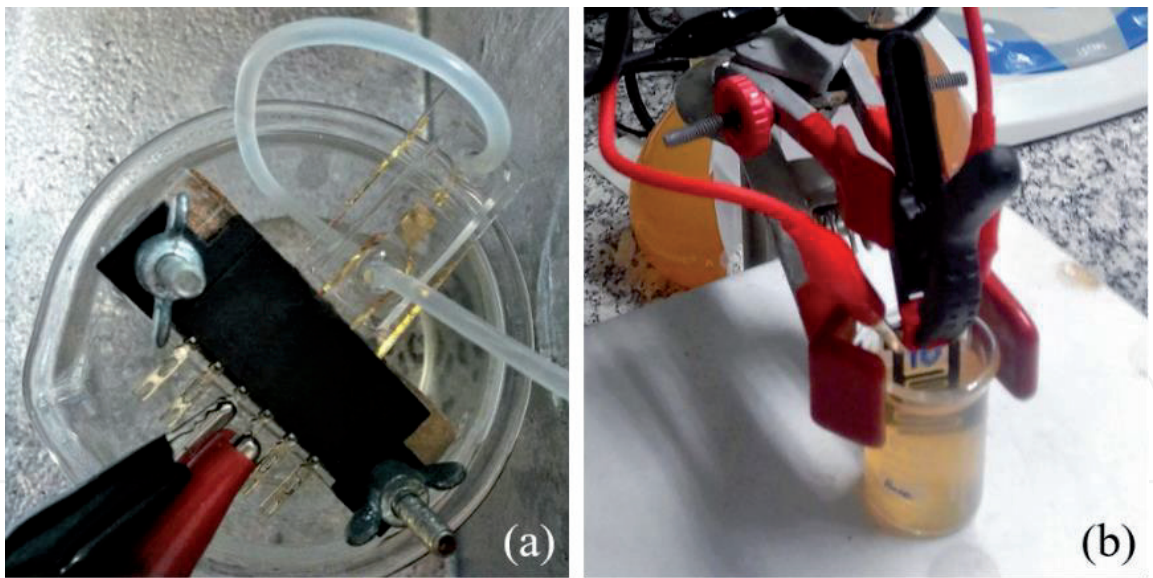


Figure 7. Different devices used as sensing units for *e-tongue* system in soil analysis: (a) gold IDE inside a PDMS microchannel and (b) graphene-based 3D-printed IDE.

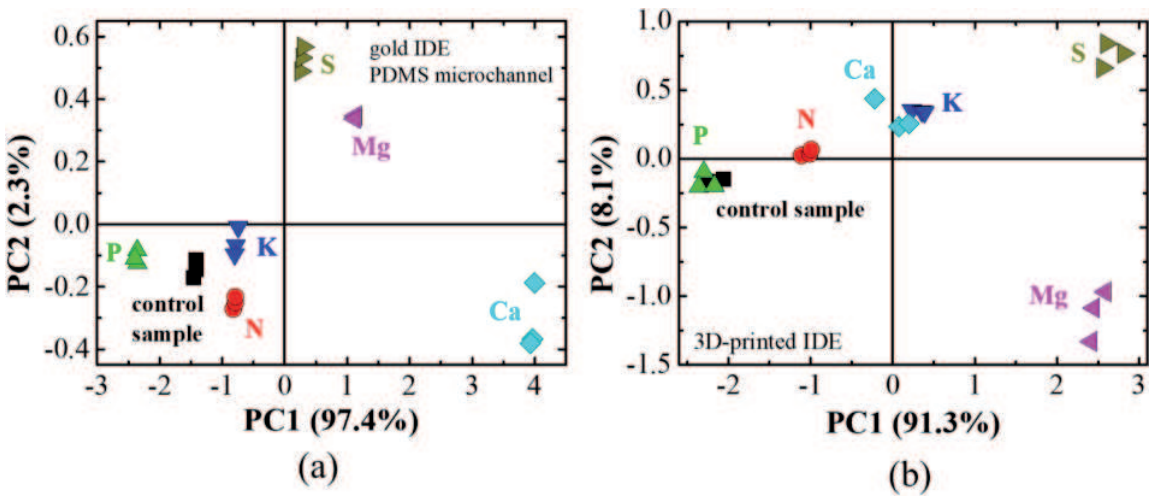


Figure 8. PCA for the 1 kHz capacitance results of the *e-tongue* systems on (a) microfluidic and (b) on 3D-printed electrodes, both applied in soil samples diluted in water (control, N, P, K, Ca, Mg, and S).

samples using the 3D-printed electrodes was observed (**Figure 8b**), which does not occur with the conventional device (**Figure 8a**) fabricated with gold IDEs and PDMS microchannels. However, considering the contribution of the third main Principal Component (PC3), all the samples could also be easily separated with the 3D-printed device [24].

3. Conclusions

The LbL technique is a striking research line in materials science based on nanostructured films fabricated from distinct building blocks (polymers, organic macromolecules, clays, and reduced graphene oxides). The molecular level thickness control offered by the LbL assembly enables multilayered nanostructures exhibiting interesting assignments in numerous applications. The use of physical methods to controllably embed metallic nanoparticles into LbL films is an interesting alternative approach to give a better understanding of modifications introduced

in hybrid materials. Overall, the use of LbL films in sensing applications requires previous electrode fabrication, and within this context we have compared gold IDEs manufactured by photolithography with 3D-printed electrodes using a graphene-based filament. The 3D-printing technique also enables the successful integration of e-tongue devices into microfluidic systems, reducing processing steps and costs. Devices fabricated by different methods show pros and cons, and the decision of which one to use depends on the application, budget, and time available. Therefore, an e-tongue multisensory system was used to illustrate the application of multilayered thin films in the analysis of soil samples enriched with plant macronutrients, by comparing electrodes manufactured by both conventional methods (photolithography) and an emergent technology (3D-printing). The 3D-printing technology has proved to be an interesting approach in integrating different areas such as microfluidics, sensing, and electrode manufacturing, with a reduction in costs, processing steps, and manufacturing time, expanding at the same time novel opportunities in sensorial analysis.

Acknowledgements

The authors are grateful for the financial support from the Brazilian funding agencies: Sao Paulo Research Foundation (FAPESP, grants no 2015/14836-9 and 2017/19862-3), Coordination for the Improvement of Higher Education Personnel (CAPES), and National Council for Scientific and Technological Development (CNPq). They also thank the Brazilian Nanotechnology National Laboratory (LNNano)/National Center for Research in Energy and Materials (CNPEM) (LMF project n° 24749) for providing photolithography facilities.

Conflict of interest


The authors declare no conflict of interest.

Author details

Maria L. Braunger, Rafael C. Hensel, Gabriel Gaál, Mawin J.M. Jimenez, Varlei Rodrigues and Antonio Riul Jr*
Department of Applied Physics, “Gleb Wataghin” Institute of Physics (IFGW), University of Campinas (UNICAMP), Campinas, SP, Brazil

*Address all correspondence to: riul@ifi.unicamp.br

IntechOpen

© 2020 The Author(s). Licensee IntechOpen. Distributed under the terms of the Creative Commons Attribution - NonCommercial 4.0 License (<https://creativecommons.org/licenses/by-nc/4.0/>), which permits use, distribution and reproduction for non-commercial purposes, provided the original is properly cited. 

References

- [1] Iler RK. Multilayers of colloidal particles. *Journal of Colloid and Interface Science*. 1966;**21**:569-594. DOI: 10.1016/0095-8522(66)90018-3
- [2] Decher G. Fuzzy nanoassemblies: Toward layered polymeric multi-composites. *Science*. 1997;**277**:1232-1237. DOI: 10.1126/science.277.5330.1232
- [3] Richardson JJ, Björnmalm M, Caruso F. Technology-driven layer-by-layer assembly of nanofilms. *Science*. 2015;**348**:2491. DOI: 10.1126/science.aaa2491
- [4] Richardson JJ, Cui J, Björnmalm M, et al. Innovation in layer-by-layer assembly. *Chemical Reviews*. 2016;**116**:14828-14867. DOI: 10.1021/acs.chemrev.6b00627
- [5] Zhao S, Caruso F, Dähne L, et al. The future of layer-by-layer assembly: A tribute to ACS Nano associate editor Helmuth Möhwald. *ACS Nano*. 2019;**13**:6151-6169. DOI: 10.1021/acsnano.9b03326
- [6] Alessio P, Constantino CJL, Daikuzono CM, et al. Analysis of coffees using electronic tongues. In: Mendez MR, editor. *Electronic Noses and Tongues in Food Science*. Oxford, UK: Academic Press; 2016. pp. 171-177
- [7] Daikuzono CM, Shimizu FM, Manzoli A, et al. Information visualization and feature selection methods applied to detect Gliadin in gluten-containing foodstuff with a microfluidic electronic tongue. *ACS Applied Materials & Interfaces*. 2017;**9**:19646-19652. DOI: 10.1021/acsami.7b04252
- [8] Salvo-Comino C, García-Hernández C, García-Cabezón C, Rodríguez-Méndez ML. Discrimination of milks with a multisensor system based on layer-by-layer films. *Sensors*. 2018;**18**:1-12. DOI: 10.3390/s18082716
- [9] de Barros A, Constantino CJL, da Cruz NC, et al. High performance of electrochemical sensors based on LbL films of gold nanoparticles, polyaniline and sodium montmorillonite clay mineral for simultaneous detection of metal ions. *Electrochimica Acta*. 2017;**235**:700-708. DOI: 10.1016/j.electacta.2017.03.135
- [10] Andre RS, Shimizu FM, Miyazaki CM, et al. Hybrid layer-by-layer (LbL) films of polyaniline, graphene oxide and zinc oxide to detect ammonia. *Sensors Actuators, B Chem*. 2017;**238**:795-801. DOI: 10.1016/j.snb.2016.07.099
- [11] Rodrigues GHS, Miyazaki CM, Rubira RJG, et al. Layer-by-layer films of Graphene Nanoplatelets and gold nanoparticles for methyl parathion sensing. *ACS Appl Nano Mater*. 2019;**2**:1082-1091. DOI: 10.1021/acsanm.9b00007
- [12] World Health Organization. Available from: www.who.int
- [13] de Lucena NC, Miyazaki CM, Shimizu FM, et al. Layer-by-layer composite film of nickel phthalocyanine and montmorillonite clay for synergistic effect on electrochemical detection of dopamine. *Applied Surface Science*. 2018;**436**:957-966. DOI: 10.1016/j.apsusc.2017.12.117
- [14] Camilo DE, Miyazaki CM, Shimizu FM, Ferreira M. Improving direct immunoassay response by layer-by-layer films of gold nanoparticles – Antibody conjugate towards label-free detection. *Materials Science and Engineering: C*. 2019;**102**:315-323. DOI: 10.1016/j.msec.2019.04.055

- [15] Silva DPB, Miyazaki CM, Mascagni DBT, Ferreira M. Layer-by-layer films of gold nanoparticles and carbon nanotubes for improved Amperometric detection of cholesterol. *Journal of Nanoscience and Nanotechnology*. 2019;**19**:5483-5488. DOI: 10.1166/jnn.2019.16534
- [16] Fontinele LP, de Sousa RC, Viana VGF, et al. Norbixin extracted from urucum (*Bixa orellana* L.) for the formation of conductive composites with potential applications in electrochemical sensors. *Surfaces and Interfaces*. 2018;**13**:92-100. DOI: 10.1016/j.surfin.2018.08.002
- [17] Cortez ML, Lorenzo A, Marmisollé WA, et al. Highly-organized stacked multilayers: Via layer-by-layer assembly of lipid-like surfactants and polyelectrolytes. Stratified supramolecular structures for (bio) electrochemical nanoarchitectonics. *Soft Matter*. 2018;**14**:1939-1952. DOI: 10.1039/c8sm00052b
- [18] Cummins G, Desmulliez MPY. Inkjet printing of conductive materials: A review. *Circuit World*. 2012;**38**:193-213. DOI: 10.1108/03056121211280413
- [19] Singh M, Haverinen HM, Dhagat P, Jabbour GE. Inkjet printing-process and its applications. *Advanced Materials*. 2010;**22**:673-685. DOI: 10.1002/adma.200901141
- [20] Paula KT, Gaál G, Almeida GFB, et al. Femtosecond laser micromachining of polylactic acid/graphene composites for designing interdigitated microelectrodes for sensor applications. *Optics and Laser Technology*. 2018;**101**:74-79. DOI: 10.1016/j.optlastec.2017.11.006
- [21] Canessa E, Fonda C, Zennaro M. Low-Cost 3D Printing for Science, Education & Sustainable Development. Trieste, It: ICTP Science Dissemination Unit; 2013
- [22] Gaal G, Mendes M, de Almeida TP, et al. Simplified fabrication of integrated microfluidic devices using fused deposition modeling 3D printing. *Sensors and Actuators B: Chemical*. 2017;**242**:35-40. DOI: 10.1016/j.snb.2016.10.110
- [23] Foster CW, Down MP, Yan Z, et al. 3D printed Graphene based energy storage devices. *Scientific Reports*. 2017;**7**:1-11. DOI: 10.1038/srep42233
- [24] Gaál G, Silva TA, Gaál V, et al. 3D printed e-tongue. *Frontiers in Chemistry*. 2018;**6**:151. DOI: 10.3389/fchem.2018.00151
- [25] Sharma S, Shriwastava S, Kumar S, et al. Alternative transparent conducting electrode materials for flexible optoelectronic devices. *Opto-electronics Rev*. 2018;**26**:223-235. DOI: 10.1016/j.opelre.2018.06.004
- [26] Lee HB, Jin WY, Ovhal MM, et al. Flexible transparent conducting electrodes based on metal meshes for organic optoelectronic device applications: A review. *Journal of Materials Chemistry C*. 2019;**7**:1087-1110. DOI: 10.1039/c8tc04423f
- [27] Li Y, Xu G, Cui C, Li Y. Flexible and semitransparent organic solar cells. *Advanced Energy Materials*. 2018;**8**:1-28. DOI: 10.1002/aenm.201701791
- [28] Koo JH, Kim DC, Shim HJ, et al. Flexible and stretchable smart display: Materials, fabrication, device design, and system integration. *Advanced Functional Materials*. 2018;**28**:1-23. DOI: 10.1002/adfm.201801834
- [29] Ellmer K. Past achievements and future challenges in the development of optically transparent electrodes. *Nature Photonics*. 2012;**6**:809-817. DOI: 10.1038/nphoton.2012.282
- [30] Wang DH, Kyaw AKK, Gupta V, et al. Enhanced efficiency parameters

of solution-processable small-molecule solar cells depending on its sheet resistance. *Advanced Energy Materials*. 2013;**3**:1161-1165. DOI: 10.1002/aenm.201300277

[31] Sakamoto K, Kuwae H, Kobayashi N, et al. Highly flexible transparent electrodes based on mesh-patterned rigid indium tin oxide. *Scientific Reports*. 2018;**8**:3-4. DOI: 10.1038/s41598-018-20978-x

[32] Hecht DS, Hu L, Irvin G. Emerging transparent electrodes based on thin films of carbon nanotubes, graphene, and metallic nanostructures. *Advanced Materials*. 2011;**23**:1482-1513. DOI: 10.1002/adma.201003188

[33] Ok KH, Kim J, Park SR, et al. Ultra-thin and smooth transparent electrode for flexible and leakage-free organic light-emitting diodes. *Scientific Reports*. 2015;**5**:1-8. DOI: 10.1038/srep09464

[34] Zhang C, Khan A, Cai J, et al. Stretchable transparent electrodes with solution-processed regular metal mesh for an electroluminescent light-emitting film. *ACS Applied Materials & Interfaces*. 2018;**10**:21009-21017. DOI: 10.1021/acsami.8b06691

[35] Ji Y, Yang J, Luo W, et al. Ultraflexible and high-performance multilayer transparent electrode based on ZnO/Ag/CuSCN. *ACS Applied Materials & Interfaces*. 2018;**10**:9571-9578. DOI: 10.1021/acsami.7b15902

[36] Altin Y, Tas M, Borazan I, et al. Solution-processed transparent conducting electrodes with graphene, silver nanowires and PEDOT: PSS as alternative to ITO. *Surf Coatings Technol*. 2016;**302**:75-81. DOI: 10.1016/j.surfcoat.2016.05.058

[37] Singh V, Joung D, Zhai L, et al. Graphene based materials: Past, present

and future. *Progress in Materials Science*. 2011;**56**:1178-1271. DOI: 10.1016/j.pmatsci.2011.03.003

[38] Jimenez MJM, de Oliveira RF, Shimizu FM, et al. Poole-Frenkel emission on functionalized, multilayered-packed reduced graphene oxide nanoplatelets. *Nanotechnology*. 2018;**29**:505703. DOI: 10.1088/1361-6528/aae18e

[39] Wang Y, Li Z, Wang J, et al. Graphene and graphene oxide : Biofunctionalization and applications in biotechnology. *Trends in Biotechnology*. 2011;**29**:205-212. DOI: 10.1016/j.tibtech.2011.01.008

[40] Li D, Müller MB, Gilje S, et al. Processable aqueous dispersions of graphene nanosheets. *Nature Nanotechnology*. 2008;**3**:101-105. DOI: 10.1038/nnano.2007.451

[41] Diao S, Zhang X, Shao Z, et al. 12.35% efficient Graphene quantum dots/silicon Heterojunction solar cells using Graphene transparent electrode. *Nano Energy*. 2017;**31**:359-366. DOI: 10.1016/j.nanoen.2016.11.051

[42] Lee T, Min SH, Gu M, et al. Layer-by-layer assembly for Graphene-based multilayer Nanocomposites : Synthesis and applications. *Chemistry of Materials*. 2015;**27**(11):3785-3796. DOI: 10.1021/acs.chemmater.5b00491

[43] Morales-Narváez E, Merkoçi A. Graphene oxide as an optical biosensing platform: A Progress report. *Advanced Materials*. 2019;**31**:1-12. DOI: 10.1002/adma.201805043

[44] Kruk T, Socha RP, Szyk-Warszyńska L, Warszyński P. Flexible and ultrathin polyelectrolyte conductive coatings formed with reduced graphene oxide as a base for advanced new materials. *Applied Surface Science*. 2019;**484**:501-510. DOI: 10.1016/j.apsusc.2019.04.051

- [45] Tian P, Tang L, Teng KS, Lau SP. Graphene quantum dots from chemistry to applications. *Mater Today Chem.* 2018;**10**:221-258. DOI: 10.1016/j.mtchem.2018.09.007
- [46] Krishnan SK, Singh E, Singh P, et al. A review on graphene-based nanocomposites for electrochemical and fluorescent biosensors. *RSC Advances.* 2019;**9**:8778-8781. DOI: 10.1039/c8ra09577a
- [47] Jimenez MJM, Oliveira RF, Almeida TP, et al. Charge carrier transport in defective reduced graphene oxide as quantum dots and nanoplatelets in multilayer films. *Nanotechnology.* 2017;**28**:495711. DOI: 10.1088/1361-6528/aa91c2
- [48] Jimenez MJM, de Oliveira RF, Bufon CCB, et al. Enhanced mobility and controlled transparency in multilayered reduced graphene oxide quantum dots: A charge transport study. *Nanotechnology.* 2019;**30**:275701. DOI: 10.1088/1361-6528/ab118e
- [49] Schöning MJ, Poghossian A, Yoshinobu T, Lüth H. Semiconductor-based field-effect structures for chemical sensing. *Adv Environ Chem Sens Technol.* 2001;**4205**:188-198. DOI: 10.1117/12.417449
- [50] Poghossian A, Abouzar MH, Amberger F, et al. Field-effect sensors with charged macromolecules: Characterisation by capacitance-voltage, constant-capacitance, impedance spectroscopy and atomic-force microscopy methods. *Biosensors & Bioelectronics.* 2007;**22**:2100-2107. DOI: 10.1016/j.bios.2006.09.014
- [51] Abouzar MH, Poghossian A, Razavi A, et al. Characterisation of capacitive field-effect sensors with a nanocrystalline-diamond film as transducer material for multi-parameter sensing. *Biosensors & Bioelectronics.* 2009;**24**:1298-1304. DOI: 10.1016/j.bios.2008.07.056
- [52] Poghossian A, Abouzar MH, Sakkari M, et al. Field-effect sensors for monitoring the layer-by-layer adsorption of charged macromolecules. *Sensors and Actuators B.* 2006;**118**:163-170. DOI: 10.1016/j.snb.2006.04.013
- [53] Poghossian A, Weil M, Cherstvy AG, Schöning MJ. Electrical monitoring of polyelectrolyte multilayer formation by means of capacitive field-effect devices. *Analytical and Bioanalytical Chemistry.* 2013;**405**:6425-6436. DOI: 10.1007/s00216-013-6951-9
- [54] Hensel RC, Rodrigues KL, Pimentel V do L, et al. Automated self-assembly and electrical characterization of nanostructured films. *MRS Commun.* 2018;**8**:283-288. DOI: 10.1557/mrc.2018.47
- [55] Han JT, Zheng Y, Cho JH, et al. Stable superhydrophobic organic-inorganic hybrid films by electrostatic self-assembly. *The Journal of Physical Chemistry. B.* 2005;**109**:20773-20778. DOI: 10.1021/jp052691x
- [56] Sato K, Takahashi S, Anzai J. Layer-by-layer thin films and microcapsules for biosensors and controlled release. *Analytical Sciences.* 2012;**28**:929-938. DOI: 10.2116/analsci.28.929
- [57] Khillan RK, Su Y, Lvov YM, Varshramyan K. Layer-by-layer nanoarchitecture of ultrathin films of PEDOT-PSS and PPy to act as hole transport layer in polymer light emitting diodes and polymer transistors. *IEEE Trans Components Packag Technol.* 2005;**28**:748-753. DOI: 10.1109/TCAPT.2005.859754
- [58] Mercante LA, Scagion VP, Pavinatto A, et al. Electronic tongue based on nanostructured hybrid films of

- gold nanoparticles and Phthalocyanines for Milk analysis. *Journal of Nanomaterials*. 2015;**2015**:1-7. DOI: 10.1155/2015/890637
- [59] Ravagnan L, Divitini G, Rebasti S, et al. Poly(methyl methacrylate)-palladium clusters nanocomposite formation by supersonic cluster beam deposition: A method for microstructured metallization of polymer surfaces. *Journal of Physics D: Applied Physics*. 2009;**42**:082002. DOI: 10.1088/0022-3727/42/8/082002
- [60] de Sá ADT, Abrao Oiko VT, di Domenicantonio G, Rodrigues V. New experimental setup for metallic clusters production based on hollow cylindrical magnetron sputtering. *J Vac Sci Technol B, Nanotechnol Microelectron Mater Process Meas Phenom*. 2014;**32**:061804. DOI: 10.1116/1.4900847
- [61] Blaiszik BJ, Kramer SLB, Olugebefola SC, et al. Self-healing polymers and composites. *Annual Review of Materials Research*. 2010;**40**:179-211. DOI: 10.1002/9781118082720
- [62] Ai H, Jones SA, Lvov YM. Biomedical applications of electrostatic layer-by-layer Nano-assembly of polymers, enzymes, and nanoparticles. *Cell Biochemistry and Biophysics*. 2003;**39**:23-43
- [63] Wijeratne S, Liu W, Dong J, et al. Layer-by-layer deposition with polymers containing Nitrilotriacetate, a convenient route to fabricate metal- and protein-binding films. *ACS Applied Materials & Interfaces*. 2016;**8**:10164-10173. DOI: 10.1021/acsami.6b00896
- [64] Tang Z, Kotov NA, Magonov S, Ozturk B. Nanostructured artificial nacre. *Nature Materials*. 2003;**2**:413-418. DOI: 10.1038/nmat906
- [65] Hager MD, Greil P, Leyens C, et al. Self-healing materials. *Advanced Materials*. 2010;**22**:5424-5430
- [66] Xiang Z, Zhang L, Yuan T, et al. Healability demonstrates enhanced shape-recovery of Graphene-oxide-reinforced shape-memory polymeric films. *ACS Applied Materials & Interfaces*. 2018;**10**:2897-2906. DOI: 10.1021/acsami.7b14588
- [67] Vidyasagar A, Sung C, Gamble R, Lutkenhaus JL. Thermal transitions in dry and hydrated layer-by-layer assemblies exhibiting linear and exponential growth. *ACS Nano*. 2012;**6**:6174-6184. DOI: 10.1021/nn301526b
- [68] Chen XC, Ren KF, Zhang JH, et al. Humidity-triggered self-healing of microporous polyelectrolyte multilayer coatings for hydrophobic drug delivery. *Advanced Functional Materials*. 2015;**25**:7470-7477. DOI: 10.1002/adfm.201503258
- [69] Mishra P, Mapara S, Vyas P. Testing/monitoring of soil chemical level using wireless sensor network technology. *Int J Appl or Innov Eng Manag*. 2015;**4**:114-117
- [70] Rogovska N, Laird DA, Chiou CP, Bond LJ. Development of field mobile soil nitrate sensor technology to facilitate precision fertilizer management. *Precision Agriculture*. 2019;**20**:40-55. DOI: 10.1007/s11119-018-9579-0
- [71] Hartemink AE, McBratney AB. *Proximal Soil Sensing*. New York, USA: Springer; 2010
- [72] Braunger ML, Shimizu FM, Jimenez MJM, et al. Microfluidic electronic tongue applied to soil analysis. *Chem*. 2017;**5**:1-10. DOI: 10.3390/chemosensors5020014